Facile synthesis of PVDF/SnO_2 nanocomposite thin films for optoelectronic applications

S. A. Hafeez[a], M. Saleem[b], U. Waqas[a,*], N. Ather[c], S. M. Ramay[d], M. A. Shar[e], S. Atiq[a]

[a]*Centre of Excellence in Solid State Physics, University of the Punjab, Lahore 54590, Pakistan*
[b]*Department of Physics, School of Science and Engineering (SSE), Lahore University of Management Sciences (LUMS), Lahore, Pakistan*
[c]*Institute of Physics, Islamia University Bahawalpur, Pakistan*
[d]*Department of Physics and Astronomy, King Saud University (KSU), Riyadh, Saudi Arabia*
[e]*Department of Mechanical & Energy Systems Engineering, Faculty of Engineering and Informatics, University of Bradford, Bradford BD7 1DP, United Kingdom*

Thin films of pure polyvinylidene fluoride (PVDF) and PVDF/SnO_2 nanocomposites were fabricated by sol− gel spin coating method. The weight percentage of SnO_2 in PVDF matrix was varied from 0.25%, 0.5%, and 1%. X-ray diffraction graphs exhibited the rutile structure of SnO_2. Scanning electron microscope confirmed densely packed morphology of pure PVDF and dispersion of SnO_2 agglomerated spherical particles in PVDF matrix. The presence of all constituent elements in a specific ratio was confirmed from energy-dispersive X-ray spectroscopy. Furthermore, optical properties were taken by ellipsometry in terms of ψ (Psi) and Δ (Delta) values which were acquired through the specific fitting model, and these modeled values were fitted with the experimental values. The real part of the dielectric function showed a high refractive index at minimum energy for pure PVDF as compared to PVDF/SnO_2 nanocomposite films whereas the imaginary part exhibited significantly high absorption spectra at minimum energy for pure PVDF and vice versa for PVDF/SnO_2 films. Furthermore, pure PVDF film showed high absorption which increased with the increase of energy of interacting light but decreased with the incorporation of SnO_2 nanoparticles. The entire observation exhibited that PVDF/SnO_2 nanocomposite thin films can be utilized for optical devices like transpicuous conductors and chemical sensors etc.

(Received May 17, 2024; Accepted September 2, 2024)

Keywords: PVDF, Transparent semiconductors, Rutile structure, Ellipsometry

1. Introduction

Transparent semiconductors are at the heart of the optical industry because of their applications in various devices like photodetectors, photovoltaic cells, and liquid crystal displays [1]. Generally, a number of semiconducting oxides have been extensively used for these applications [2]. Tin oxide (SnO_2) is a unique wide bandgap (3.4 eV) semiconducting material with high optical transparency (≥85%) and n-type carriers [3]. In addition, it is non-toxic, environmentally friendly, has high chemical and electrical stability with low cost of production. Electrical conductions of SnO_2 stem over the native and foreign oxygen vacancies which generate extra energy levels in bandgap and thus facilitate the conduction phenomenon. Therefore, SnO_2 has low resistivity (3.71×10^{-1} Scm^{-1}) and high carrier concentration (5.5×10^{-18} cm^{-3}) as compared with other transparent conducting materials [4]. Furthermore, optical transparent nature in the visible range of wavelength and simplest noncubic structure with no orbital complications make it

* Corresponding author: umerwaqas149@gmail.com
https://doi.org/10.15251/JOR.2024.205.579

an exceptional choice for display devices like transpicuous conductors, light-emitting diode, gas sensors in microelectronics, anti-reflective coatings on the top of solar cells, and electrochemical detectors [4]

Owing to the wide spectrum of applications of SnO_2 based composite, a lot of work has been devoted to synthesize their thin films using different deposition techniques such as aerosol assisted chemical vapor deposition [6], sol-gel technique [7], chemical spray pyrolysis technique [8], RF magnetron sputtering technique [9], electron beam evaporation [10], chemical vapor deposition technique [11], etc. Among all these techniques, low processing cost, cheap apparatus used, and time efficiency make the sol-gel method advantageous It is the better choice to synthesized pure and dopes metal oxides because it provides good control over stoichiometry and crustal structure growth.

The next-generation electronic industry relies on flexible and optically transparent materials in the visible range of wavelength which could be achieved by making the composites of optically transparent semiconductors with polymer matric. Due to this reason, nano-composite thin films of transparent semiconducting material have gained much attention [12]. However, the mixing of inorganic semiconducting compounds in polymer matrix produces surprising results which improve optical characteristics of nanocomposite thin films significantly [13, 14]. Therefore, the potential of such nanocomposites thin films for optoelectronic devices is the main reason for their exploration in the last few years.

Few reports revealed that the introduction of SnO_2 nanoparticles into the PVDF matrix can increase its optical and electronic properties which motivated us to explore the optical behavior of PVDF/SnO_2 nanocomposite thin films to check their potential for next-generation optoelectronic devices [15]. Therefore, this work intends to characterize the PVDF/SnO_2 nanocomposite thin films with different concentrations (0.25%, 0.5% & 1%) of SnO_2 in pure PVDF matrix which were successfully prepared onto a p-type silicon substrate by sol-gel method using spin coating technique. The structural, morphological, elemental, and optical properties of pure PVDF and PVDF/SnO_2 nanocomposite thin films were studied by X-ray diffraction (XRD), scanning electron microscopy (SEM), energy-dispersive X-ray spectroscopy (EDX), and spectroscopy ellipsometry (SE).

2. Experimental

2.1. Preparation of PVDF/SnO_2 nanocomposites

Before the nanocomposite synthesis, SnO_2 nanoparticles were synthesized separately using the sol-gel auto-combustion technique. In this technique, the calculated amount of $Sn(CH_3CO_2)_2$ was dissolved in 100 ml distilled water to prepare a 0.01 M solution and put on the hot plate. Then a fixed amount of citric acid $(C_6H_8O_7).H_2O$ was added to this solution as a fuel agent and the temperature of the hot plate was adjusted to 80 ^oC to form (gel). After few hours when gel became sufficiently thick, the temperature was increased by 250 ^oC which caused auto combustion. This combustion turned the viscous solution into powder form. The obtained powder was thermally treated at 600 ^oC for 4 h to get a fine crystalline form of tin oxide (SnO_2) nanoparticles. The synthesis procedure of SnO_2 nanoparticles can be seen in Figure 1(a).

To prepare PVDF/SnO_2 nanocomposite thin films for next-generation flexible electronic components we dissolved a particular amount of PVDF powder into a specific quantity of N, N-dimethylformamide (DFM). Then, we added a desire concentration (0.25wt.%, 0.5wt.% & 1wt.%) of SnO_2 nano-particles into this solution. This solution was heated at 50 ^oC for 6 h for the preparation of PVDF/SnO_2 nanocomposite thin films. The p-type silicon was used as a substrate to deposit the nanocomposite thin films with the help of a commercial spin coater as shown in Figure 1(b). Before depositing nanocomposite thin film, all the substrates were chemically cleaned and dried with the N_2 gun. After that, the substrate was fixed on the rotator of the spin coater one by one and kept the speed at 4000 rpm for 30 sec. Then all the prepared PVDF/SnO_2 nanocomposite thin films were cooled at room temperature.

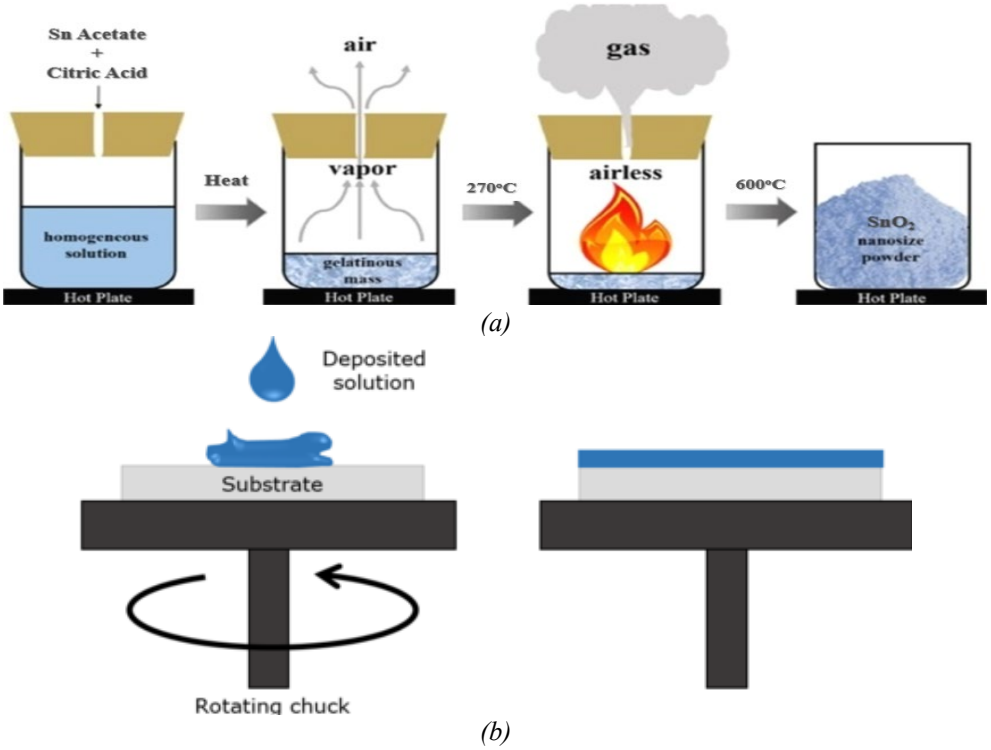

Fig. 1. (a) Schematic of Auto-Combustion method and (b) Sol-Gel Spin Coater.

3. Results and discussion

3.1. Structural analysis

Figure 2 shows the XRD patterns of pure PVDF and PVDF/SnO_2 nanocomposite thin films of various concentrations (0.25%, 0.5% & 1%) of SnO_2 nano-particles. For the polymer structure of pure PVDF, the peaks in the diffraction pattern were noticed at 2θ values of 18.82°, 37.00°, 43.20°, and 76.62° respectively which belong to the β-phase of PVDF.

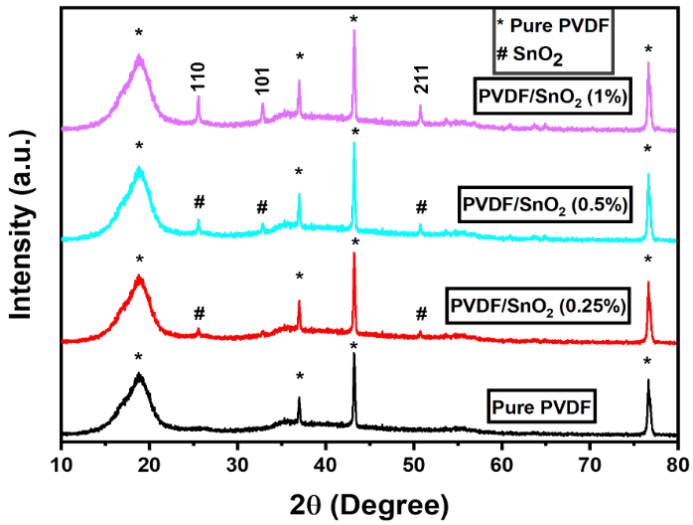

Fig. 2. XRD patterns of pure PVDF and PVDF/SnO_2 nanocomposite thin films.

The peaks in the diffracted pattern of PVDF/SnO_2 nanocomposites film were observed at 2θ values of 25.64°, 32.82°, 50.78°, 60.94°, 63.46°, and 64.86° which corresponds to the (110), (101), (211), (310), (112) and (301) planes respectively and belong to the rutile phase of SnO_2. The formation of the rutile phase of SnO_2 was confirmed by matching these peaks with JCPDS card no. 01-072-1147. The calculated values of lattice constant were $a = b = 4.71$ Å and $c = 3.86$ Å. It has been observed that the intensity of peaks belonging to the rutile phase of SnO_2 is enhanced as the concentration of SnO_2 increases from 0.25 wt.% to 1 wt.%. In addition, the calculated values of crystallite size (2.294-3.690 nm) and micro-strain are summarized in Table 1. Thus, the presence of peaks belongs to PVDF and the rutile phase of SnO_2 provide quite convincing evidence regarding the formation of PVDF/SnO_2 nanocomposites.

Table 1. Crystallite size and micro strain of pure PVDF and PVDF/SnO_2 thin films.

Thin Films	Crystallite Size (D) (nm)	Micro Strain (ε)
Pure PVDF	2.294	0.565
PVDF/SnO_2 (0.25%)	1.943	0.432
PVDF/SnO_2 (0.5%)	1.950	0.436
PVDF/SnO_2 (1%)	3.690	0.324

3.2. Morphology analysis

Figure 4 represents the different features of the SEM images of pure PVDF and PVDF/SnO_2 nanocomposite thin films at a magnification of 100,000x. The arbitrary and spherulite-shaped particles with agglomeration were found in Figure 3(a). The average particle size of pure PVDF is 78 nm. The PVDF's surface topography consists of numerous spherulites because PVDF is a polymer that is semicrystalline in nature [16]. On the other hand, all PVDF/SnO_2 nanocomposite thin films show spherical nanocrystalline grains which are randomly dispersed in the PVDF matrix which can be seen in Figure 3(b), (c) & (d). The particle size is mentioned in the SEM images.

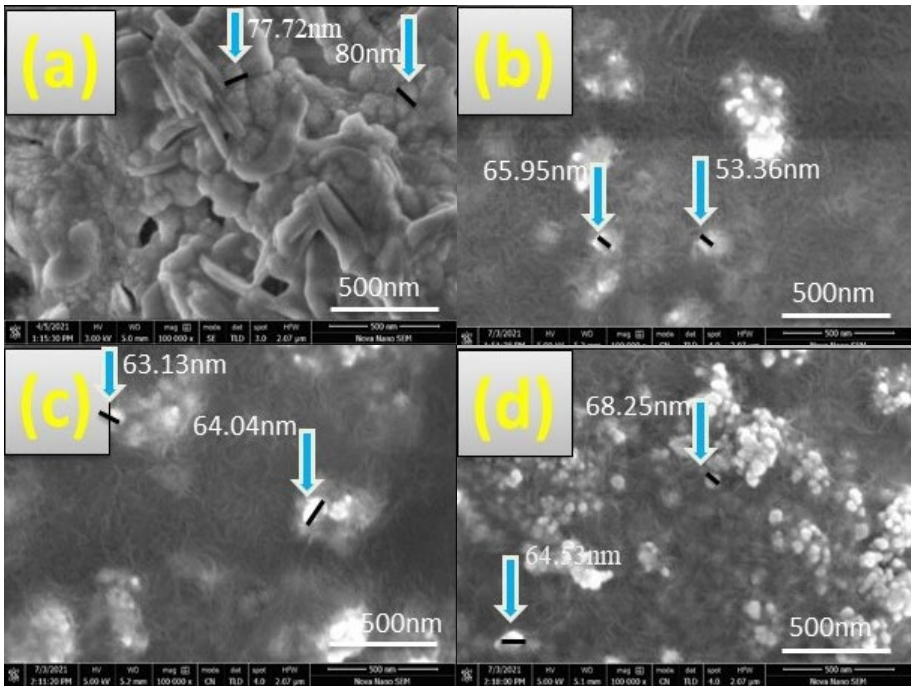

Fig. 3. SEM images of (a) PVDF, PVDF/SnO_2 composites with (b) 0.25 wt.%, (c) 0.50 wt.% and (d) 1 wt.% SnO_2 in PVDF matrix obtained at a magnification of x100,000.

3.3. Compositional analysis

Figure 4 represents the EDX spectra of pure PVDF and PVDF/SnO_2 nanocomposite thin films with different concentrations of SnO_2. It confirms the presence of SnO_2 nanoparticles and determines their weight percentage (wt.%). Figure 4(a) shows the EDX spectrum of 0.25% SnO_2 in PVDF where all peaks belong to the elements such as fluorine (F), carbon (C), tin (Sn), and oxygen (O) with respective elemental percentages. Similarly, Figures 4(b) & (c) confirm the preparation of PVDF/SnO_2 nanocomposite thin films with 0.5% and 1% of SnO_2 by the existence of respective elements. Where Si peak came from the substrate. Hence, the substitution of SnO_2 in PVDF was affirmed. The weight percent of all elements in nanocomposite thin films are shown in Table 2.

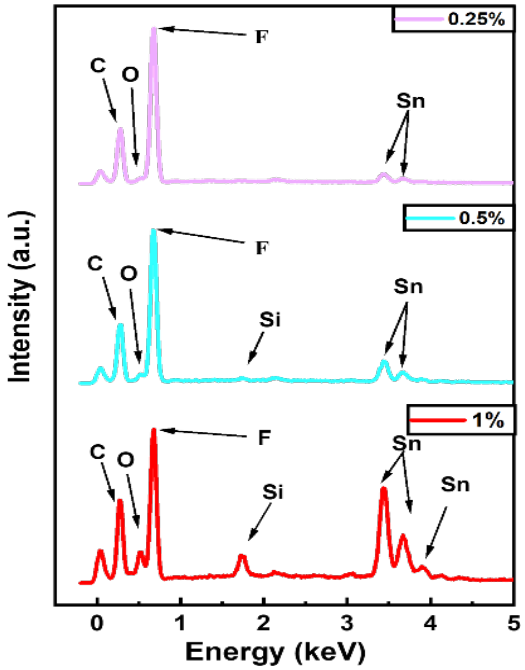

Fig. 4. EDX Spectra of PVDF/SnO_2 nanocomposite thin film with 0.25, 0.5 & 1 wt.% of SnO_2 in composite.

Table 2. Elemental Composition of PVDF/SnO2 nanocomposite thin films.

Wt.% of SnO_2 in PVDF	Wt.% Sn	Wt.% F	Wt.% O	Wt.% C	Wt.% Si
0.25	8.72	60.08	1.83	29.37	-
0.50	16.35	55.22	2.97	25.10	0.36
1.00	35.64	37.82	7.51	17.42	1.61

3.4. Optical analysis

Characterization of the optical response of the material is vital before using it for optical devices. The optical response of pure PVDF and PVDF/SnO_2 nanocomposite was analyzed using spectroscopic ellipsometry. It is used to observe the optical behavior of pure PVDF and PVDF/SnO_2 nanocomposite thin films of different wt.% (0.25%, 0.5% & 1%) of SnO_2 nanoparticles. The optical parameters are associated through a ratio between r_s and r_p as given in Eq. 1.

$$\rho = \frac{r_p}{r_s} \times \tan\Psi e^{i\Delta} \quad (1)$$

The ellipsometry technique is generally composed of two components (s & p) which are parallel and perpendicular and that's normally created after the polarization of light when it strikes with the material. A light in which $\bar{E}$ aligned to an incident dimension and magnetic field is perpendicular to that incident light and vice versa for S-polarized light. By using Eq.1, two parameters, amplitude ratio (ψ) and angle/phase shift (Δ) are set up from which all optical properties are extracted. A root means square error (MSE) is used to observe how much the experimental values are matched with the built-in ellipsometry model as shown in Eq. 2 [17].

$$\mathrm{MSE} = \sqrt{\frac{1}{3m-1}\sum_{i=1}^{m}(N_{Ei} - N_{Ci})^2 + (C_{Ei} - C_{Ci})^2 + (S_{Ei} - S_{Ci})^2} \times 1000 \quad (2)$$

In this equation m is the total no. of measured wavelengths, $C = \sin 2\Psi \cos \Delta$, $N = \cos 2\Psi$ and $S = \sin 2\Psi \sin \Delta$.

The Cauchy model is applied to derive the optical properties which are related to the phase shift (Δ) and the amplitude ratio (Ψ). For obtaining these properties, place a thin film in ellipsometry spectroscopy for the analysis by a given light source that falls on the film at a specific angle within a particular energy regime. Figure 5 shows the experimental fitting lines and model fitting lines for obtaining Psi (Ψ) and Delta (Δ) graphs with energy. Figure 5(a) shows the fitting graph of pure PVDF for the analysis of Ψ/Δ which shows that there is not a good agreement between the experimental values and model data. With the addition of 0.25% and 0.5%, SnO_2 nano-particles to pure PVDF, the agreement between theoretical and experimental results increased as shown in Figure 5(b) & (c), respectively. But in Figure 5(d) Ψ/Δ plot, it can be seen that there is a very good fitting agreement which appeared by incorporation of 1% concentration of SnO_2 nano-particles. From all the films, Figure 5(d) showed the best fit with the model.

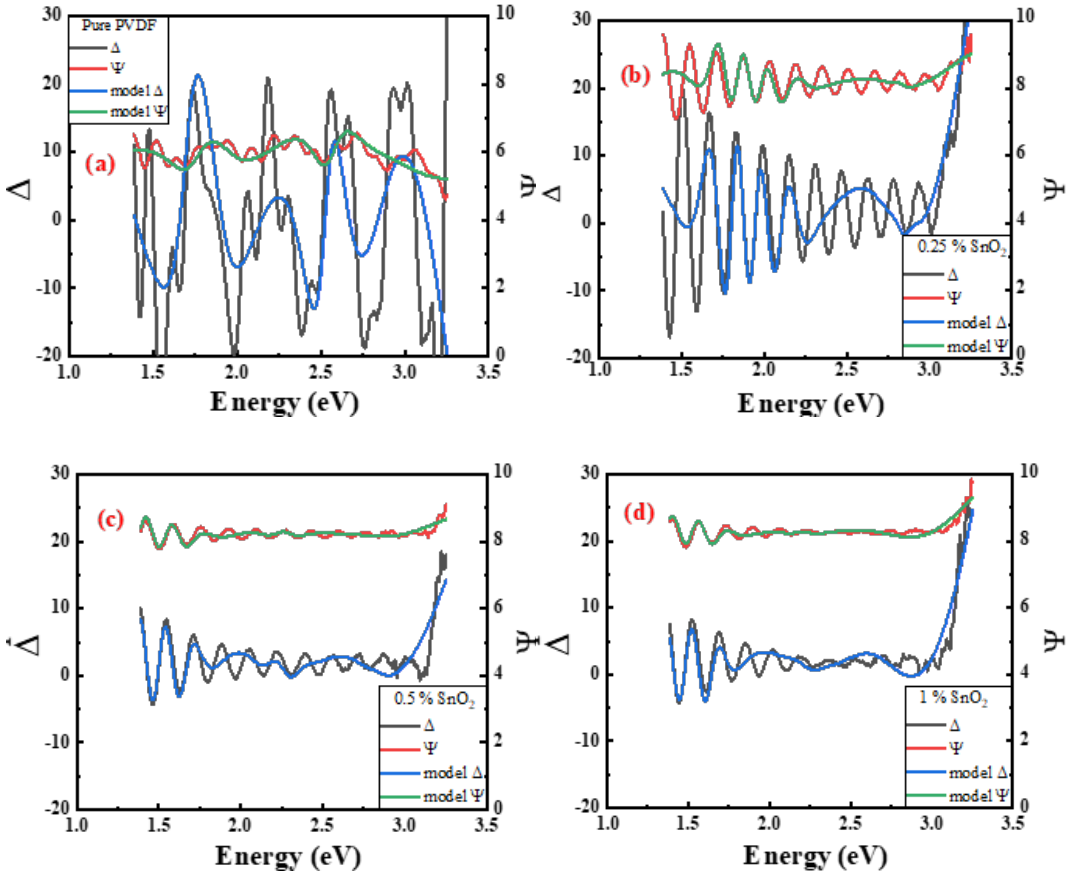

Fig. 5. ψ, Δ plot of the ellipsometry graph for (a) pure PVDF (b) 0.25 % SnO_2, (c) 0.5 % SnO_2 and (d) 1% SnO_2.Figure 6(a) shows the plot of refractive index (n) of pure PVDF and PVDF/SnO_2 nanocomposite thin films.

The pure PVDF shows the value of the refractive index of 1.95 at minimum energy of 1.38 eV, upon increasing energy it shows variation with increasing energy up to 3.25 eV. An introduction of 0.25% concentration of SnO_2 shows a decrease in the value of *n* as compared to pure PVDF film. However, when the concentration of SnO_2 was increased to 0.5% & 1% in the nanocomposite thin films the fluctuation in the value of the refractive index decreased significantly and became an almost stable value in the range of energy 1.5-3 eV. When the energy of incident light increases beyond 3 eV, the value of *n* for all compositions is sharply reduced which shows that all these compositions are transparent in near IR and visible region of light. Variation in extinction coefficient (κ) with the energy of an incident photon is shown in Figure 6(b). The figure shows that the value of κ for pure PVDF is 0.3 cm^{-1} at minimum energy and reaches a maximum value at 0.48 cm^{-1} at high energy 3 eV after a huge dip. After reaching the maximum, the value κ again starts decreasing. When the concentration of SnO_2 is introduced and then increased all-composite thin films exposed the same trend i.e., attenuation increased sharply when the energy of incident light is increased from 2.9 eV.

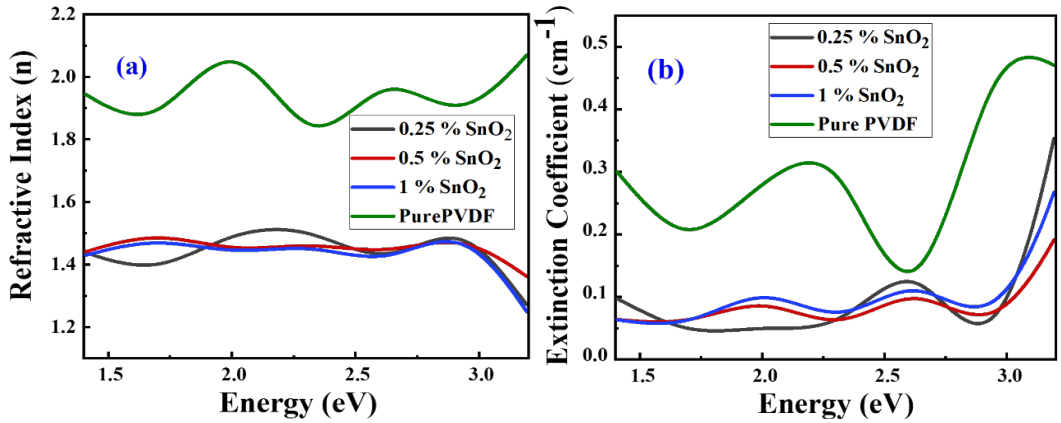

Fig. 6. Variation in (a) refractive index (n) and (b) the extinction coefficient (k) vs energy (eV) for 0.25%, 0.5% & 1% of SnO_2 and pure PVDF.

Using the values of κ and *n*, the dielectric parameters such as real part $\varepsilon_1(\omega)$ and imaginary part $\varepsilon_2(\omega)$ can be analyzed in the visible range of energy as shown in Figure 7(a) and (b). ε_1 of pure PVDF is very high and shows an almost constant value up to 2.7 eV then an increase in the energy of incident light causes an increase in ε_1.

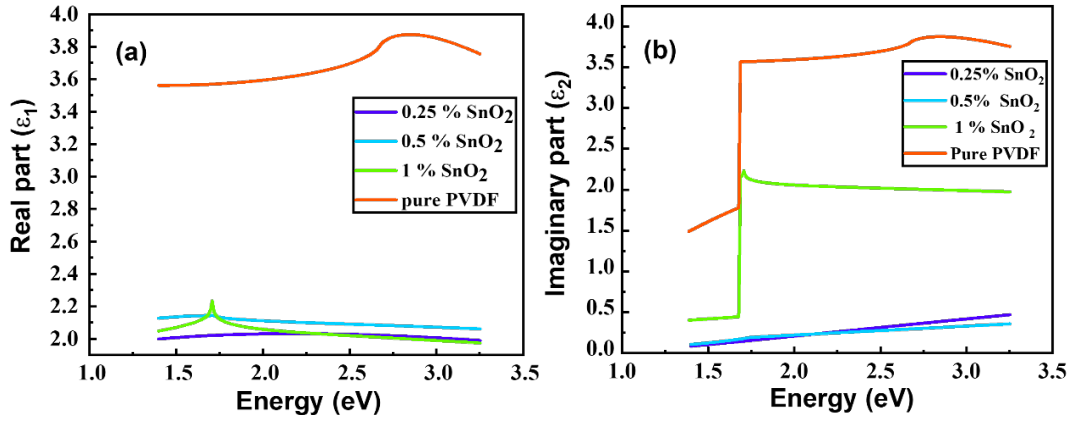

Fig. 7. Plots of (a) ε_1 real part and (b) ε_2 imaginary part of dielectric constant vs energy (eV) for 0.25%, 0.5%, 1% SnO_2 and pure PVDF.

The value of ε_1 for all composites is very low as compared to pure PVDF and remains almost constant in the full energy range. The composition with 1% SnO_2 revealed a peak at 1.7 eV which may be attributed to the relaxation process associated with the SnO_2 semiconductors.

The absorbance graph of pure PVDF and PVDF/SnO_2 nanocomposite thin films is shown in Figure 8(a). It can be seen from the graph that pure PVDF thin film has sufficiently high absorption in near IR and visible spectra which exhibited that it is a good absorber while PVDF/SnO_2 nanocomposite thin films have relatively low absorption in the same region. It is clear from the figure that all nanocomposite thin films are transparent for the visible and near IR region. Figure 8(b) shows the reflected intensity of pure PVDF and PVDF/SnO_2 nanocomposite thin films. The reflective intensity of pure PVDF is highest among all these compositions and varies with the energy of incident radiation. The maximum reflection intensity is noticed at 2.5 eV which rapidly decreased when energy is further increased. This shows that pure PVDF film has good reflectivity in the visible region as well as near IR region while all nanocomposite thin films show low reflectance in the same spectrum.

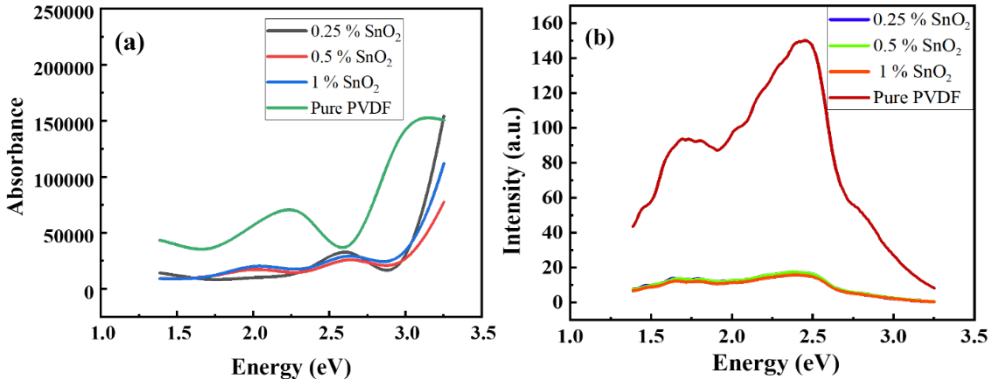

Fig. 8. Variation in (a) absorbance spectra (α) and (b) the intensity (arb. units) vs energy (eV) for 0.25%, 0.5%, 1% SnO2 and pure PVDF

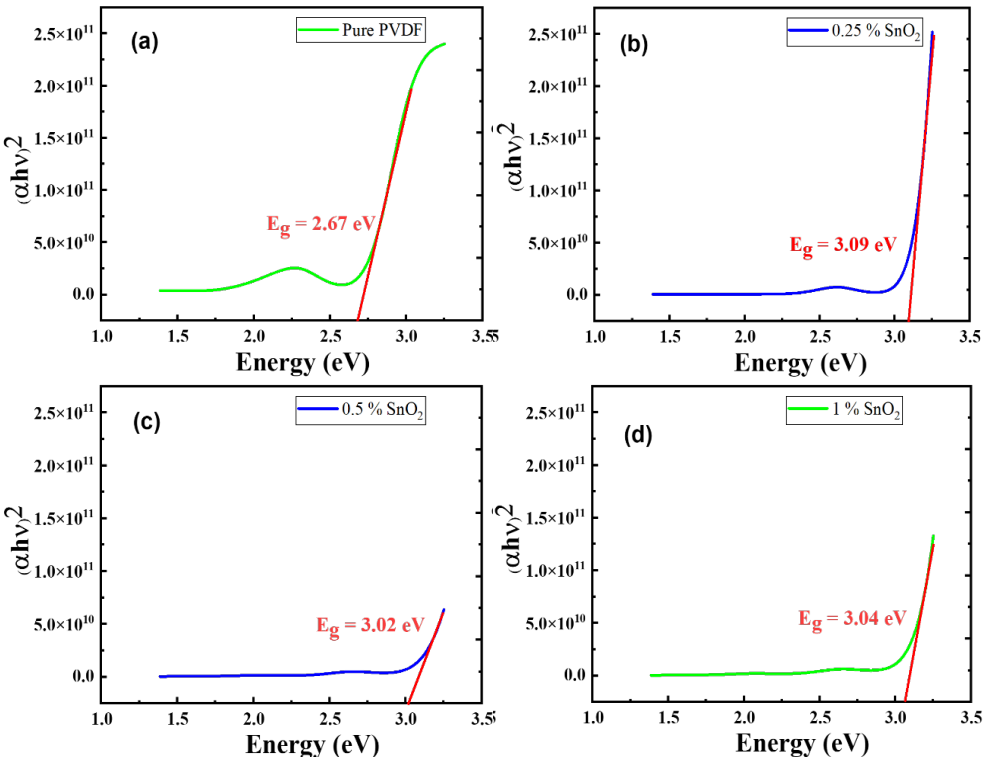

Fig. 9. Band gap $(ahv)^2$ vs energy (eV) for (a) pure PVDF (b) 0.25% SnO_2, (c) 0.5% SnO_2, and (d) 1% SnO_2.

Among the optical parameters, the energy bandgap is a key factor that was calculated using Tauc relation and plotted against the energy of incident radiation as shown in Figure 9. This figure shows the variation of $(\alpha h\upsilon)^2$ vs energy (eV) which gives information about the bandgap (E_g) of the pure PVDF thin film and PVDF/SnO_2 nanocomposites. The value of E_g is about 2.67 eV for pure PVDF as shown in Figure 9(a). This bandgap has increased to 3.09 eV with the addition of 0.25% SnO_2 nanoparticles as shown in Figure 9(b). However, the remaining two nanocomposite thin films show a bandgap between the pure PVDF and PVDF/SnO_2 (0.25%) such as 3.02 eV and 3.04 eV respectively which can be seen in Figure 9(c & d).

4. Conclusion

Here we synthesized optically transparent semiconductor (SnO_2) based nanocomposites thin films using a spin-coating technique. SnO_2 nanoparticles synthesized using the sol-gel auto-combustion route were added to the PVDF matrix by varying its weight percentage as 0.25%, 0.5%, and 1%. Structural investigations revealed the presence of β-phase of PVDF and rutile phase of SnO_2 which confirmed the formation of PVDF/SnO_2 nanocomposites. The value of lattice parameters for SnO_2 particles was noticed as $a = b = 4.71$ Å and $c = 3.86$ Å while the value of crystallite size was in the range of 2.294-3.690 nm. Wight percentage of all elements present in the composites matched with their stoichiometric calculations and thus confirmed the formation of PVDF/SnO_2 composites.

Morphological analysis revealed the dispersion of spherical grains of SnO_2 in the PVDF matrix and the average particle size of these particles was 65 nm. Using ellipsometry the optical parameters like refractive index, extinction coefficient, the real and imaginary part of dielectric constant with absorbance and reflectance were plotted in the visible range of energy. These results revealed that the addition of SnO_2 particles in the PVDF matrix reduced the refractive index, extinction coefficient, and absorption intensity. These results highlight the importance of these composite thin films for transparent semiconducting devices.

Acknowledgement

The authors would like to acknowledge the Researchers Supporting Project number (RSP2024R71), King Saud University, Riyadh, Saudi Arabia.

References

[1] H. He, Z. Yang,Y. Xu, A. T. Smith, G. Yang, L. Sun, Nano Convergence, 7(1),(2020), 1-10; https://doi.org/10.1186/s40580-020-00242-7

[2] R. A. Afre, N. Sharma, M. Sharon, M. Sharon, Reviews on advanced materials science,53(1), (2018), 79-89; https://doi.org/10.1515/rams-2018-0006

[3] B. Babu, I. N. Reddy, K. Yoo, D. Kim, J. Shim, Materials Letters, 221, (2018), 211-215; https://doi.org/10.1016/j.matlet.2018.03.107

[4] R. Mientus, M. Weise, S. Seeger, R. Heller, K. Ellmer, Coatings, 10(3), (2020), 204; https://doi.org/10.3390/coatings10030204

[5] M. Bhatnagar, V. Kaushik, A. Kaushal, M. Singh, B. R. Mehta, AIP Advances, 6(9), (2016),095321; https://doi.org/10.1063/1.4964313

[6] S. M. Ali, S. T. Hussain, S. A. Bakar, J. Muhammad, N. Ur-Rehman, Journal of Physics: Conference Series (Vol. 439, No. 1, p. 012013). IOP Publishing; https://doi.org/10.1088/1742-6596/439/1/012013

[7] M. Shaban, G. F. Attia, M. A. Basyooni, H. Hamdy, Journal of Modern Trends in Physics Research, 14, (2014), 90-99; https://doi.org/10.19138/MTPR/(14)90-99

[8] N. A. Bakr, S. A. Salman, M. N. Ali, Advances in Materials, 5(4), (2016), 23-30; https://doi.org/10.11648/j.am.20160504.12

[9] A. Alhuthali, M. M. El-Nahass, A. A. Atta, M. M. Abd El-Raheem, K. M. Elsabawy, A. M. Hassanien, Journal of Luminescence, 158, (2015), 165-171; https://doi.org/10.1016/j.jlumin.2014.09.044

[10] J. C. Jiang, K. Lian, E. I. Meletis, Thin Solid Films, 411(2), (2002), 203-210; https://doi.org/10.1016/S0040-6090(02)00288-2

[11] C. F. Wan, E. D. McGrath, W. F. Keenan, S. N. Frank, Journal of the Electrochemical Society, 136(5), (1989), 1459; https://doi.org/10.1149/1.2096941

[12] B. A. Rozenberg, R. Tenne, Progress in Polymer Science, 33(1), (2008), 40-112; https://doi.org/10.1016/j.progpolymsci.2007.07.004

[13] M. Z. Rong, M. Q. Zhang, Y. X. Zheng, H. M. Zeng, R. Walter, K. Friedrich, Journal of Materials Science Letters, 19(13), (2000), 1159-1161; https://doi.org/10.1023/A:1006711326705

[14] O. I. Dimitry, Z. I. Abdeen, E. A. Ismail, A. L. G. Saad, Journal of Polymer Research, 17(6), (2010), 801-813; https://doi.org/10.1007/s10965-009-9371-y

[15] M. Haridas, S. Srivastava, J. K. Basu, Bulletin of Material Science, 31(3), (2008), 213-217; https://doi.org/10.1007/s12034-008-0038-9

[16] V. Bharti, R. Nath, Journal of Physics D: Applied Physics, 34(5), (2001), 667; https://doi.org/10.1088/0022-3727/34/5/301

[17] C. Yim, M. O'Brien, N. McEvoy, S. Winters, I. Mirza, J. G. Lunney, G. S. Duesberg,. Applied Physics Letter, 104(10), (2014), 103114; https://doi.org/10.1063/1.4868108